Journal of Hazardous Materials 168 (2009) 747–752

Contents lists available at ScienceDirect

Journal of Hazardous Materials

journal homepage: www.elsevier.com/locate/jhazmat

Size effects of nanocrystalline TiO_2 on As(V) and As(III) adsorption and As(III) photooxidation

Zhonghou Xu, Xiaoguang Meng*

Center for Environmental Systems, Stevens Institute of Technology, Hoboken, NJ 07030, USA

ARTICLE INFO

Article history:
Received 19 August 2008
Received in revised form
29 December 2008
Accepted 16 February 2009
Available online 25 February 2009

Keywords:
TiO_2
Arsenate
Arsenite
Adsorption
Size effect
Photooxidation

ABSTRACT

The physicochemical properties of TiO_2 particles in the diameter range between 6.6 and 30.1 nm and the effect of the crystalline size on arsenic adsorption and photocatalytical oxidation were investigated. TiO_2 nanoparticles of different sizes were single-phase anatase. The adsorption capacity of the TiO_2 for As(III) and As(V) increased linearly with the N_2 Brunauer–Emmett–Teller surface area (S_{BET}) of the particles. There was not much difference in the rate of As(III) photooxidation when the diameter of the TiO_2 nanoparticles was between 6.6 and 14.8 nm. However, the As(III) photooxidation rate clearly decreased when the particle size increased to 30.1 nm. Arsenite photooxidation data could be fitted with a first-order kinetics equation.

Published by Elsevier B.V.

1. Introduction

Arsenic is one of the most toxic contaminants found in the environment and has been recognized as a toxic element for centuries. Arsenic contamination has caused severe health problems, such as skin, lung, urinary bladder, liver and kidney cancers, especially in some developing countries where a significant percentage of the population depends on groundwater for drinking. High-As groundwater areas have been found in Argentina, Chile, Mexico, China, Hungary, West Bengal (India), Bangladesh and Vietnam [1].

Arsenic exists in the −3, 0, +3 and +5 oxidation states. Pentavalent species predominate and are stable in oxygen-rich aerobic environments, while trivalent arsenites predominate in moderately reducing anaerobic environments, such as groundwater. Several treatment techniques are available for removing arsenic from water, such as adsorption, coagulation/precipitation, ion exchange, lime softening, reverse osmosis and electrodialysis [2,3]. Numerous studies have been conducted to assess the removal capacity of adsorbents [3]. Most technologies require pre-oxidation of As(III) to As(V) to enhance removal of As(III), since As(V) adsorbs more strongly onto the solid phase than As(III). As(III) oxidation is carried out by oxidants, such as chlorine compounds, ozone, H_2O_2, and Fenton's reagent [4,5].

The oxidation of As(III) to As(V) can also be accomplished by photocatalytic reactions using TiO_2 as a catalyst [6–13]. The commonly used TiO_2 in research was a commercial product Degussa P25 [11–13], which is about 30 nm in particle size and is a mixture of about 80% anatase and 20% rutile. Nanocrystalline TiO_2 is effective in the photocatalytic oxidation of As(III) and for adsorption of As(V) and As(III) [14,15]. The adsorption capacity of nanocrystalline TiO_2 for As(V) and As(III) was much higher than fumed TiO_2 (Degussa P25) [14]. Bang et al. [15] reported that approximately 45,000 bed volumes of groundwater containing an average of 39 μg/L of As(V) was treated by the point-of-entry filter filled with nanocrystalline TiO_2 before the effluent arsenic concentration increased to 10 μg/L.

The size effect is important on the adsorption and photoactivity of TiO_2 nanoparticles [16–20]. Zhang et al. [16] reported that when the TiO_2 particle size decreases from 6 to <1.4 nm, physical adsorption and hydrogen bonding forms of adsorbed carboxylate decrease from 36% to 3%, whereas chemical binding forms increase from 74% to 97%. The primary crystal size of photocatalysts determines both the photo-conversion efficiency and the specific surface area, which are essential to a good photocatalyst. Several experiments indicated that an optimum particle size of TiO_2 exists such that the photocatalytic oxidation rates of organic substrates are maximized [18,19].

Although several studies have been conducted to assess the size-dependent effect on photocatalytic reactivity of TiO_2 nanoparticles, most research has focused on the photooxidation of organic compounds, such as trichloroethylene [18], phenol [19], rhodamine B

* Corresponding author. Tel.: +1 201 2168014; fax: +1 201 2188303.
E-mail address: xmeng@stevens.edu (X. Meng).

0304-3894/$ – see front matter. Published by Elsevier B.V.
doi:10.1016/j.jhazmat.2009.02.084

[20] and methylene blue dye [21]. In this study, the physicochemical properties of TiO_2 nanoparticles with different sizes were systematically characterized. The size effects of TiO_2 nanoparticles on As(V) and As(III) adsorption and As(III) photooxidation were investigated.

2. Materials and methods

2.1. Materials and chemicals

All solutions were prepared using A.C.S. certificated chemicals and deionized water (DI). Stock solutions of 1000 mg-As/L of arsenic were prepared using sodium salt heptahydrate ($Na_2HAsO_4{\cdot}7H_2O$) and sodium arsenite ($NaAsO_2$).

The nanocrystalline TiO_2 was produced by hydrolysis of titanium sulfate solution [22]. The pH of the slurry was adjusted to a range between 4 and 9 with sodium hydroxide, and the slurry was filtered to collect the titanium dioxide solids. The titanium dioxide solids were washed with water to remove salts, then were dried at 105 °C for 2 h. Samples of the dried titanium dioxide product were sieved to obtain a 100-standard U.S. mesh fraction. The material in powder form costs less than commercial granular ferric hydroxide (GFH) and granular ferric oxide (GFO) [14]. Other TiO_2 samples of different size were prepared by calcining the above nanocrystalline TiO_2 at 200, 350, 500, and 700 °C for 3 h.

2.2. Sample characterization

X-ray diffraction patterns of the sample powders were recorded using an Ultima IV Goniometer 285 mm System using Cu Kα radiation at a 2θ scan rate of $0.02^\circ\ s^{-1}$. The data were used for crystal phase identification, and the crystallite size (Φ) was estimated from the Scherrer formula: $\Phi = K\lambda/(\beta\cos\theta)$, where λ is the wavelength of the X-ray radiation (0.154 nm), K is usually taken as 0.89 [23], β is the peak width at half-maximum height after subtraction of the equipment broadening, $2\theta = 25.3^\circ$ for TiO_2 in the anatase form.

The morphology and grain size of the TiO_2 samples were examined by transmission electron microscopy (Philips CM20 TEM). Raman spectra of the TiO_2 powders were scanned using a Nicolet Almega XR Dispersive Raman Spectrometer. The laser wavelength was 780 nm, power was 35 mW, and resolution was 1.9–2.3 cm^{-1}. The N_2 BET surface area was determined using a Micrometrics ASAP 2100. The pore volume was the single point adsorption total pore volume of pores less than 707.9 Å at P/P_0 of 0.97.

An acid–base titration method was used to determine the surface hydroxyl density in accordance with Sigg and Stumm [24]. Briefly, a 100 mL suspension of 10 g/L TiO_2 was created in pure Millipore DI water. The pH of the suspension was adjusted to pH 3.0 using HCl. Then the mixture was purged for 2 h with N_2 gas to remove dissolved carbonate. After purging, the suspension pH was raised to the PZC of 5.8 [14], and allowed to rest for 24 h. The suspension was assumed to be in complete equilibrium, and an excess amount of HCl was added and allowed to saturate the suspension for another 24 h. When completely saturated, the solids in suspension were separated from the solution with a 0.2-μm membrane filter, and the supernatant was then back-titrated to pHpzc with NaOH. The surface hydroxyl density was calculated by subtracting the number of moles of the back titrant, NaOH, from the initial number of moles of HCl added, and dividing the result by the weight of TiO_2 in the suspension.

2.3. As(III) and As(V) adsorption

To evaluate TiO_2 size effects on As(III) and As(V) removal, batch experiments were done in spiked aged tap water, with an initial arsenic concentration of 50 mg-As/L in a suspension containing 1.0 g/L TiO_2. The pH value was adjusted to 7.0 ± 0.1 by adding HCl and NaOH. After a suspension sample was mixed for 1 h, it was centrifuged at 10,000 rpm for 35 min to separate the solid from the solution.

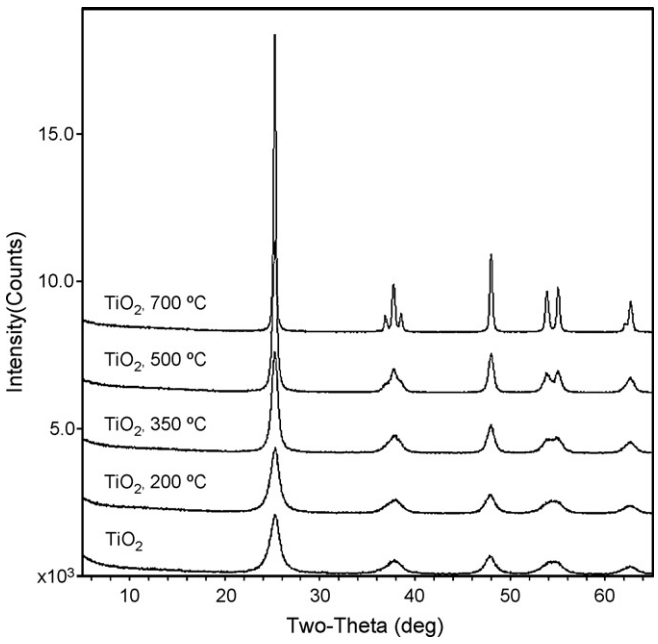

Fig. 1. XRD patterns of TiO_2 nanoparticles.

As(V) adsorption isotherms were obtained by adding different amounts of stock solutions of As(V) to a suspension containing 1.0 g/L TiO_2 and 0.04 mol/L NaCl. The pH value was adjusted to 7.0 ± 0.1 by adding HCl and NaOH at room temperature. After 24 h of mixing, the suspension was centrifuged at 10,000 rpm for 35 min to separate the solution from the solid. For As(III) adsorption isotherms, the experimental conditions were the same as for As(V) except the equilibrium time was 4 h and polyethylene terephthalate (PETE) bottles were wrapped with alumina foil to avoid As(III) oxidation [14]. Arsenic concentrations in the supernatant solution were analyzed by a Furnace atomic adsorption spectrometer (FAAS) (Varian Spectra AA-220Z).

2.4. As(III) photooxidation

As(III) photooxidation experiments were conducted with 10 mg-As/L in a suspension containing 0.02 g/L TiO_2 and 0.04 mol/L NaCl. The pH value was adjusted to 7.0 ± 0.1 by adding HCl and NaOH. The solution was illuminated with UV-light (wavelength range: 320–400 nm) using a 150 V bench Ultra Violet lamp (Model XX-15A, Spectroline Inc., California) which was placed 20 cm above the solution. At certain times, 10 mL aliquots were sampled from the suspension and were passed through an arsenic speciation cartridge packed with a 2.5 g highly selective absorbent [25]. The cartridge removed all of the arsenate, but did not remove arsenite. Then, arsenite in the filtered solution was determined using the FAAS. In general, all experiments were carefully conducted and the experimental error was about ±5%.

3. Results and discussion

3.1. Physicochemical properties of TiO_2

Fig. 1 shows the XRD patterns over a scan range from 5° to 65° 2θ for the original nanocrystalline TiO_2 and for samples calcined at 200, 350, 500 and 700 °C in air for 3 h. The XRD data for all the samples matched the standard anatase pattern (peaks at 25.3°, 37.8°,

Table 1
Characterization results of TiO_2 nanoparticles.

Sample	Crystal size (nm)	S_{BET} (m^2/g)	Pore volume[a] (cm^3/g)	Pore diameter[b] (nm)	OH density (mmol/g)	Sites (nm^{-2})
TiO_2	6.6	287.8	0.24	3.3	0.51	1.1
TiO_2, 200 °C	7.0	255.9	0.24	3.8	0.33	0.8
TiO_2, 350 °C	10.5	141.3	0.23	6.5	0.25	1.0
TiO_2, 500 °C	14.8	96.0	0.21	8.6	0.23	1.4
TiO_2, 700 °C	30.1	25.7	0.087	13.5	0.094	2.2

[a] Single point adsorption total pore volume.
[b] Adsorption average pore diameter (4 V/A by BET).

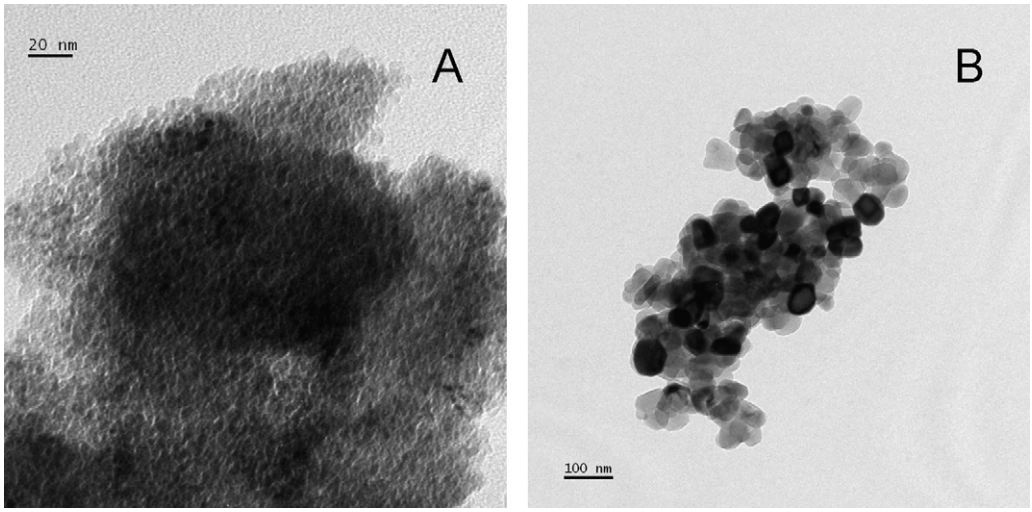

Fig. 2. TEM images of TiO_2 nanoparticles: original sample (A) and TiO_2 calcined at 700 °C (B).

47.8°, 54.5° and 62.5° 2θ). There were no diffraction peaks at 27° or 31° 2θ, indicating that the samples were free of rutile and brookite TiO_2 [26,27].

The TiO_2 samples prepared at calcination temperatures below 700 °C showed broadened diffraction peaks. The broadening effect was contributed to particle size and internal stain, which agreed with reported results [26,28,29]. The crystallite size estimated from the Scherrer formula is listed in Table 1. The primary crystal size of the original sample was 6.6 nm. As the calcination temperature increased to 200, 350, 500, and 700 °C, it enlarged to 7.0, 10.5, 14.8 and 30.1 nm. The particle size changes can also be seen from the TEM images of the original TiO_2 and the sample calcined at 700 °C in Fig. 2. The diameters of the particles determined by TEM were similar to the average particle size calculated from XRD peak broadening.

Anatase is tetragonal with the space group D194h (I41/amd). The primitive unit cell contains two TiO_2 formula units. Factor group analysis [30] indicates the existence of 15 optical modes with the following irreducible representation of normal vibrations: $1A_{1g} + 1A_{2u} + 2B_{1g} + 1B_{2u} + 3E_g + 2E_u$. The modes of A_{1g}, B_{1g} and E_g are Raman active and those of A_{2u} and E_u are infrared active. Anatase has six Raman active modes ($A_{1g} + 2B_{1g} + 3E_g$), which appear at 144 cm^{-1} (E_g), 197 cm^{-1} (E_g), 399 cm^{-1} (B_{1g}), 513 cm^{-1} (A_{1g}), 519 cm^{-1} (B_{1g}), and 639 cm^{-1} (E_g) [31].

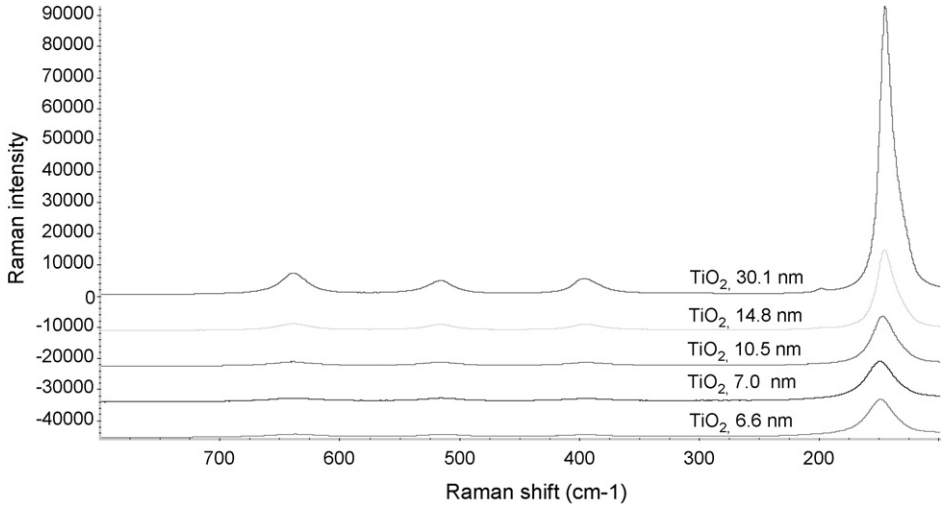

Fig. 3. Raman spectra of TiO_2 nanoparticles.

Table 2
Raman shifts of TiO_2 samples and their assignments.

Sample	E_g (high frequency)	$A_{1g} + B_{1g}$	B_{1g}	E_g (low frequency)	E_g
TiO_2	636.88	513.1	398.28		148.51
TiO_2, 200 °C	638.09	515.07	396.06		149.11
TiO_2, 350 °C	639.23	515.16	394.94		146.19
TiO_2, 500 °C	641	515.1	397.3		145.11
TiO_2, 700 °C	639.39	516.17	396.06	197.87	144.45

The Raman spectra of nanocrystalline TiO_2 samples are shown in Fig. 3 and their Raman shifts are listed in Table 2. TiO_2 nanoparticles of different sizes showed the anatase characteristic peaks at 148, 398, 513 and 636 cm^{-1}. When the calcination temperature increased to 700 °C, the intensity of these anatase peaks drastically increased, along with a red-shift (148–144 cm^{-1}) and a blue-shift (636–639 cm^{-1}) of the E_g and E_g (high frequency) modes, respectively. Band broadening and shifts of Raman bands with decreasing particle size has been investigated; the effect might be explained with a photon confinement model [32,33]. In a perfect infinite crystal only phonons close to the center of the Brillouin zone (BZ) contribute to inelastic scatterings of incident radiations. When crystal sizes range in the nanometer scale, a larger portion of the BZ is allowed to effectively participate in scattering processes due to the breakdown of the phonon momentum selection rule, i.e., $q \neq 0$ phonons can be Raman active and the phonons from the whole BZ will contribute to Raman scattering. The weight of the off-center phonons increase as the grain size decreases. The phonon dispersion causes an asymmetric broadening and the shift of the Raman peak [33,34].

The Raman spectra did not show detectable brookite or rutile. In view of the detection limit for brookite of 3.1% by XRD [35] and much less than 0.5% by Raman [36], these combined results demonstrated the formation of single-phase anatase.

Textural parameters derived from the N_2 adsorption–desorption isotherm data are summarized in Table 1. For the original TiO_2 sample, S_{BET} was 287.7 m^2/g, and the total pore volume was 0.237 cm^3/g. With increasing calcination temperature, the S_{BET} and pore volumes decreased. At 200, 350, 500 and 700 °C, the S_{BET} steadily decreased to 255.9, 141.3, 96.0 and 25.7 m^2/g, and the corresponding pore volumes decreased from 0.24 to 0.087 cm^3/g. Also, the adsorption average pore diameter of the samples increased from 3.3 to 13.5 nm as the calcination temperature increased to 700 °C. Similar changes caused by calcination have been reported [28,29]. This was due to the collapse of the pore structure and the growth of TiO_2 crystallites.

The surface hydroxyl density was determined by the acid–base titration method in accordance with Sigg and Stumm [24]. The data are listed in Table 1. The original TiO_2 had a surface –OH density of 0.51 mmol/g. As the calcining temperature increased to 200, 350, 500 and 700 °C, the –OH density decreased to 0.33, 0.25, 0.25 and 0.094 mmol/g. Regression analysis determined that the surface –OH density had a linear relationship with N_2 BET surface area (S_{BET}, m^2/g) and could described by the equation: $Y = 0.0016\ S_{BET}$ ($R^2 = 0.8219$), where Y was the surface –OH density (mmol/g).

TiO_2 –OH sites were calculated based on the surface –OH density and S_{BET} and are listed in Table 1. It can be seen that the –OH sites was about 1 nm^{-2} for all the TiO_2 samples independent of size. The differences in the data may be caused by experimental errors. This indicated that no formation of Ti-O-Ti bonds by dehydration of neighboring –OH groups occurred during the calcination process.

3.2. As(III) and As(V) adsorption

The size effects of nanocrystalline TiO_2 on As(III) and As(V) removal from spiked tap water are shown in Fig. 4. As discussed above, with increasing calcination temperature, the crystal size of TiO_2 sample increased from 6.6 to 30.1 nm. For 6.6 nm TiO_2, the As(V) adsorption was 26.5 mg-As/g under the batch experimental conditions, while for 30.1 nm TiO_2, the adsorption decreased to 1.7 mg-As/g. The removal of As(III) by the TiO_2 nanoparticles was similar to that of As(V). Under the experimental conditions, no detectable As(III) oxidation took place.

As(V) and As(III) adsorption isotherms by TiO_2 nanoparticles are shown in Fig. 5A and B, respectively. The As(III) and As(V) adsorption data can be fitted well by the Langmuir model [10,11,37]:

$$q_A = \frac{Q_M K_{ad} C_A}{(1 + K_{ad} C_A)}$$

where q_A is adsorbed arsenic in mg-As/g, C_A is the equilibrium arsenic concentration (mg-As/L), Q_M is the maximum arsenic adsorption (mg-As/g), and K_{ad} is the Langmuir adsorption constant of arsenic (L/mg).

The As(III) and As(V) adsorption parameters for the Langmuir model are listed in Table 3. Under the experimental conditions, the maximum arsenic adsorption capacity of 6.6 nm TiO_2 for As(V) was calculated by the Langmuir model to be 30.5 mg-As/g, while for the TiO_2 calcined at 200, 350, 500 and 700 °C, it decreased to 28, 18, 9.86 and 3.62 mg-As/g, respectively. The adsorption capacities of the TiO_2 for As(III) were slightly less than that for As(V).

The Q_M values of As(III) and As(V) are plotted as a function of S_{BET} of TiO_2 samples in Fig. 5C, which shows a good linear relationship. For As(V), $Q_M = 0.1096\ S_{BET}$, $R^2 = 0.9840$, while for As(III), $Q_M = 0.1018\ S_{BET}$, $R^2 = 0.9939$.

Pena et al. [14] reported that the adsorption capacity of nanocrystalline TiO_2 for As(V) and As(III) was much higher than fumed TiO_2 (Degussa P25). Mohan and Pittman [3] compared the nanocrystalline TiO_2 and other absorbents for As(V) and As(III) removal from water and wastewater.

According to the Toxicity Characteristic Leaching Procedure (TCLP) results, the spent TiO_2 generated in treatment of arsenic-contaminated groundwater was not a hazardous material [15]. But under extremely low redox potential (i.e., pe < –6), up to 38% As was

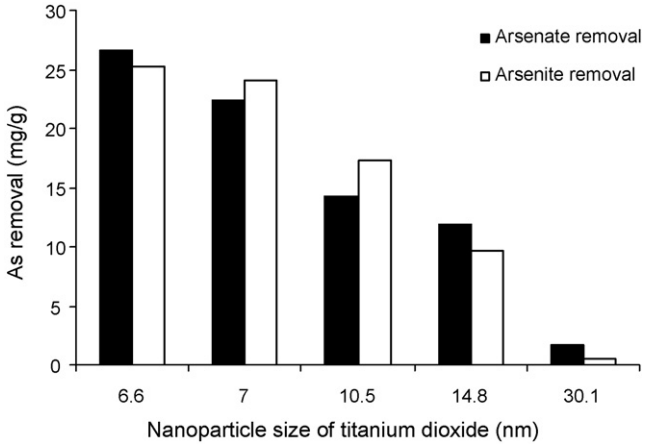

Fig. 4. Size effects of nanocrystalline TiO_2 on arsenic removal. 1 g/L TiO_2 in tap water, 50 mg-As/L, mixed for 1 h, pH 7.0 ± 0.1.

Table 3
List of Langmuir model parameters for As(III) and As(V) adsorption, and As(III) first-order photooxidation reaction parameters for TiO_2 nanoparticles.

Sample	As(V) adsorption			As(III) adsorption			As(III) photooxidation	
	Q_M (mg-As/L)	K_{ad} (L/mg)	R^2	Q_M (mg-As/L)	K_{ad} (L/mg)	R^2	$k \times 10{,}000$ (s^{-1})	R^2
TiO_2	30.5	0.33	0.9872	30.0	0.19	0.9481	3	0.9114
TiO_2, 200 °C	28.0	0.30	0.9849	25.4	0.25	0.9589	3	0.9315
TiO_2, 350 °C	18.0	0.23	0.9554	15.1	0.06	0.7971	3	0.9015
TiO_2, 500 °C	9.86	0.60	0.9824	8.52	0.24	0.9902	3	0.9164
TiO_2, 700 °C	3.62	0.12	0.8045	2.16	0.20	0.9783	0.09	0.9837

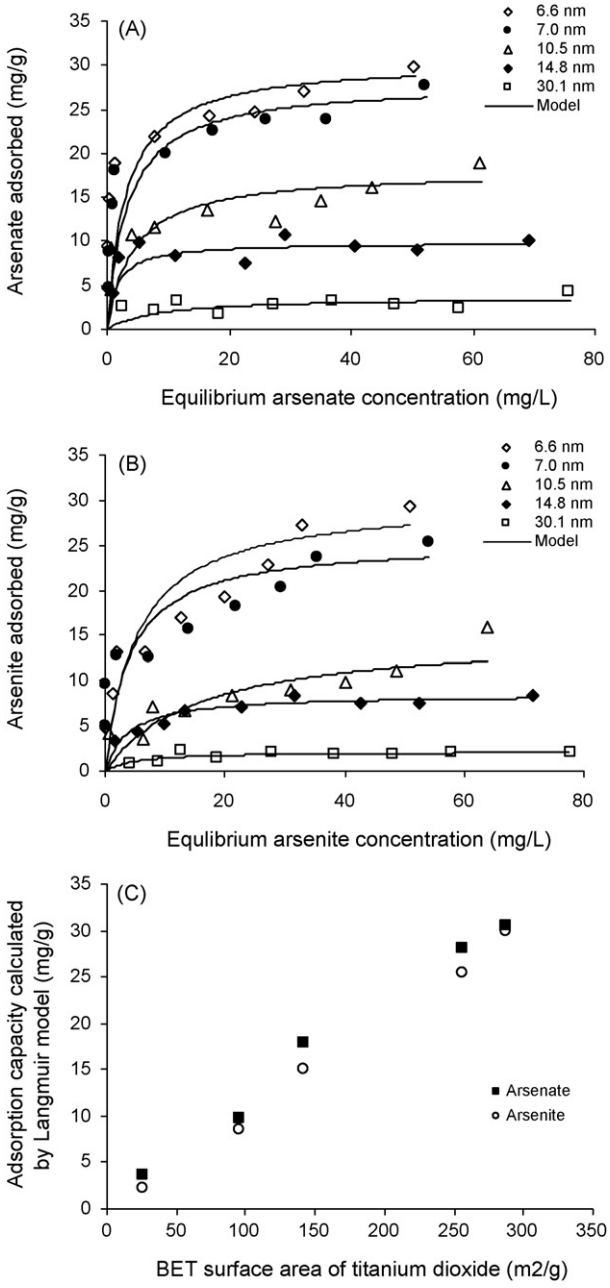

Fig. 5. (A) Arsenate adsorption isotherms on TiO_2 samples, 1 g/L TiO_2, 0.04 M NaCl, mixed for 24 h, pH 7.0 ± 0.1. (B) Arsenite adsorption isotherms on TiO_2 samples, 1 g/L TiO_2, 0.04 M NaCl, mixed for 4 h, pH 7.0 ± 0.1. (C) Linear relationship between the As adsorption capacity calculated by the Langmuir model (Q_M) and N_2 BET surface area (S_{BET}) of TiO_2 samples.

released from the spent TiO_2 adsorbent after 65 days incubation [38].

3.3. As(III) photooxidation

Photooxidation of As(III) assisted by TiO_2 of different sizes is shown in Fig. 6. For TiO_2 of 6.6 nm in diameter, the As(III) to total arsenic ratio (C/C_0) decreased rapidly from 1 to 0.15 as reaction time increased to 90 min, or about 85% of the As(III) was oxidized to As(V). Unlike the adsorption experiments described above, there was not much difference in the rate of As(III) photooxidation caused by TiO_2 nanoparticles with a diameter below 14.8 nm. However, for TiO_2 of 30.1 nm in size, the photooxidation rate clearly decreased, with about 40% As(III) oxidation in 90 min. Compared with the As(III) photooxidized by TiO_2, less than 5% of the As(III) was oxidized in the control solution without TiO_2 under UV radiation. Because of the high ratio of arsenic to TiO_2 (10 mg-As/L to 0.02 g/L), the total arsenic concentration in solution was stable. As(III) photooxidation data can be fitted with a first-order kinetics equation and the kinetic parameters are listed in Table 3. For TiO_2 with a diameter below 14.8 nm, the first-order rate constants (k) had the same value of 3×10^{-4} s^{-1}, while for 30.1 nm TiO_2, k was 9×10^{-6} s^{-1}.

Several researchers reported that an optimum particle size of TiO_2 exists such that the photocatalytic oxidation rates of organic substrates are maximized [18,19,38]. For example, Maira et al. [18] studied the photocatalytic degradation of trichloroethylene (TCE) in gas phase upon TiO_2 in the size range of 2.3 and 27 nm and reported an optimum particle size of 7 nm. Almquist and Biswas [19] reported an optimal particle size in the range of 25–40 nm with respect to photo-degradation. However, in our study for As(III) oxidation, TiO_2 photooxdition reactivity was similar when TiO_2 size was between 6.6 and 14.8 nm.

Although TiO_2 with a larger surface area should have a faster oxidation rate [17], it can be compromised by changes in band gap. TiO_2 band gap is a function of its particle size [39,40]. The band gap of ultra-fine semiconductor particles increases with decreasing

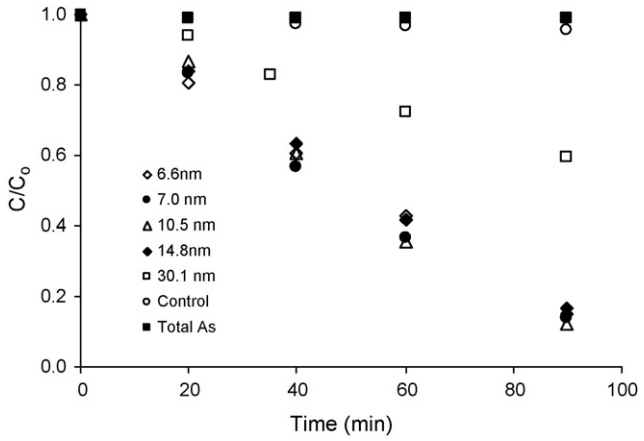

Fig. 6. Arsenite photooxidation assisted by TiO_2 of different sizes. 10 mg-As(III)/L, 0.02 g/L TiO_2, 0.04 mol/L NaCl, pH 7.0 ± 0.1.

particle size when it is smaller than the band gap minimum [41,42]. Enhancing the band gap of TiO_2 can decrease its photocatalytic performance due to less efficient utilization of lower energy photons. When TiO_2 primary crystal size decreased from 14.8 to 6.6 nm, its S_{BET} increased 141.3 to 287.7 m^2/g. To offset its S_{BET} increasing, the band gap should be increased with the primary crystal size of TiO_2 decreasing.

As indicated by Lin et al. [17] and Liu et al. [43], the combined effect of band gap change and the specific surface area (or particle size) of the TiO_2 photocatalysts determined the photocatalytic reactivity of TiO_2. This can explain why the photooxidation rate constants (k) of As(III) by TiO_2 with a size less than 14.8 nm were equal.

Other factors, such as aggregation, can affect TiO_2 photocatalytical reactivity [17,18]. Aggregation of the TiO_2 primary particles is difficult to avoid. As indicated by Maira et al. [18] and Lin et al. [17], the morphology and size of these aggregates can affect the light-scattering properties of the catalyst, but was not significantly. Further research is needed to elucidate the effect of aggregation of TiO_2 on As(III) photooxidation.

4. Conclusions

Anatase TiO_2 with particle size of about 6.6 nm was produced by hydrolysis of titanium sulfate solution, and other anatase TiO_2 samples with crystallite size of 7.0, 10.5, 14.8 and 30.1 nm were prepared by calcining the 6.6 nm TiO_2 at 200, 350, 500, and 700 °C for 3 h. With increasing size, the S_{BET}, pore volume and surface –OH density decreased, and the average pore diameter increased. The adsorption capacity of the TiO_2 for As(III) and As(V) increased linearly with the S_{BET} of the particles. There was not much difference in the rate of As(III) photooxidation when the diameter of the TiO_2 nanoparticles was between 6.6 and 14.8 nm. However, the As(III) photooxidation rate clearly decreased when the particle size increased to 30.1 nm. Based on the As(III) and As(V) adsorption and As(III) photooxidation experimental results, 6.6 nm anatase TiO_2 was more efficient for arsenic removal than the larger TiO_2 particles.

References

[1] P.L. Smedley, D.G. Kinniburgh, A review of the source, behaviour and distribution of arsenic in natural waters, Appl. Geochem. 17 (2002) 517–568.
[2] T.S.Y. Choong, T.G. Chuah, Y. Robiah, F.L.G. Koay, I. Azni, Arsenic toxicity, health hazards and removal techniques from water: an overview, Desalination 217 (2007) 139–166.
[3] D. Mohan, C.U. Pittman Jr., Arsenic removal from water/wastewater using adsorbents—a critical review, J. Hazard. Mater. 142 (2007) 1–53.
[4] J. Hug, O. Leupin, Iron-catalyzed oxidation of Arsenic(III) by oxygen and by hydrogen peroxide: ph-dependent formation of oxidants in the Fenton reaction, Environ. Sci. Technol. 37 (2003) 2734–2742.
[5] M. Pettine, L. Campanella, F.J. Millero, Arsenite oxidation by H_2O_2 in aqueous solutions, Geochim. Cosmochim. Acta 63 (1999) 2727–2735.
[6] A.L. Foster, G.E. Brown, G.A. Parks, X-ray absorption fine-structure spectroscopy study of photocatalyzed, heterogeneous As(III) oxidation on kaolin and anatase, Environ. Sci. Technol. 32 (1998) 1444–1452.
[7] M. Bissen, M. Vieillard-Baron, A.J. Schindelin, F.H. Frimmel, TiO_2-catalyzed photooxidation of arsenite to arsenate in aqueous samples, Chemosphere 44 (2001) 751–757.
[8] H. Lee, W. Choi, Photocatalytic oxidation of arsenite in TiO_2 suspension: kinetics and mechanisms, Environ. Sci. Technol. 36 (2002) 3872–3878.
[9] H. Yang, W.Y. Lin, K. Rajeshwar, Homogeneous and heterogeneous photocatalytic reactions involving As(III) and As(V) species in aqueous media, J. Photochem. Photobiol. A 123 (1999) 137–143.
[10] P.K. Dutta, A.K. Ray, V.K. Sharma, F.J. Millero, Adsorption of arsenate and arsenite on titanium dioxide suspensions, J. Colloid Interface Sci. 278 (2004) 270–275.
[11] M. Ferguson, M. Hoffmann, J. Hering, TiO_2-photocatalyzed As(III) oxidation in aqueous suspensions: reaction kinetics and effects of adsorption, Environ. Sci. Technol. 39 (2005) 1880–1886.
[12] G. Liu, X. Zhang, J.W. Talleya, C.R. Neal, H. Wang, Effect of NOM on arsenic adsorption by TiO_2 in simulated As(III)-contaminated raw waters, Water Res. 42 (2008) 2309–2319.
[13] P.K. Dutta, S.O. Pehkonen, V.K. Sharma, A.K. Ray, Photocatalytic oxidation of Arsenic(III): evidence of hydroxyl radicals, Environ. Sci. Technol. 39 (2005) 1827–1834.
[14] M.E. Pena, G.P. Korfiatis, M. Patel, L. Lippincott, X.G. Meng, Adsorption of As(V) and As(III) by nanocrystalline titanium dioxide, Water Res. 39 (2005) 2327–2337.
[15] S. Bang, M. Patel, L. Lippincott, X.G. Meng, Removal of arsenic from groundwater by granular titanium dioxide adsorbent, Chemosphere 60 (2005) 389–397.
[16] Q.L. Zhang, L.C. Du, Y.X. Weng, L. Wang, H.Y. Chen, J.Q. Li, Particle-size-dependent distribution of carboxylate adsorption sites on TiO_2 nanoparticle surfaces: insights into the surface modification of nanostructured TiO_2 electrodes, J. Phys. Chem. B 108 (2004) 15077–15083.
[17] H. Lin, C.P. Huang, W. Li, C. Ni, S.I. Shah, Y. Tseng, Size dependency of nanocrystalline TiO_2 on its optical property and photocatalytic reactivity exemplified by 2-chlorophenol, Appl. Catal. B 68 (2006) 1–11.
[18] A.J. Maira, K.L. Yeung, C.Y. Lee, P.L. Yue, C.K. Chan, Size effects in gas-phase photooxidation of trichloroethylene using nanometer-sized TiO_2 catalysts, J. Catal. 192 (2000) 185–196.
[19] C.B. Almquist, P. Biswas, Role of synthesis method and particle size of nanostructured TiO_2 on its photoactivity, J. Catal. 212 (2002) 145–156.
[20] W.C. Hao, S.K. Zheng, C. Wang, T.M. Wang, Comparison of the photocatalytic activity of TiO_2 powder with different particle size, J. Mater. Sci. Lett. 21 (2002) 1627–1629.
[21] H.D. Jang, S.J. Kim, S.K. Kim, Effect of particle size and phase composition of titanium dioxide nanoparticles on the photocatalytic properties, J. Nanoparticle Res. 3 (2001) 141–147.
[22] X.G. Meng, M. Dadachov, G.P. Korfiatis, C. Christodoulatos, Methods of preparing a surface-activated titanium oxide product and of using same in water treatment processes, U.S. Patent 6,919,029 (2005).
[23] M. Addamo, V. Augugliaro, A.D. Paola, E. García-López, V. Loddo, G. Marcì, R. Molinari, L. Palmisano, M. Schiavello, Preparation, characterization, and photoactivity of polycrystalline nanostructured TiO_2 catalysts, J. Phys. Chem. B 10 (2004) 3303–3310.
[24] L. Sigg, W. Stumm, The interaction of anions and weak acids with the hydrous goethite (a-FeOOH) surface, Colloids Surf. 2 (1981) 101–117.
[25] X.G. Meng, G.P. Korfiatis, C.Y. Jing, C. Christodoulatos, Redox transformations of arsenic and iron in water treatment sludge during aging and TCLP extraction, Environ. Sci. Technol. 35 (2001) 3476–3481.
[26] G.S. Li, L.P. Li, J. Boerio-Goates, B.F. Woodfield, High purity anatase TiO_2 nanocrystals: near room-temperature synthesis, grain growth kinetics, and surface hydration chemistry, J. Am. Chem. Soc. 127 (2005) 8659–8666.
[27] M. Pal, J. Garciá Serrano, P. Santiago, U. Pal, Size-controlled synthesis of spherical TiO_2 nanoparticles: morphology, crystallization, and phase transition, J. Phys. Chem. C 111 (2007) 96–102.
[28] S. Sivakumar, P.K. Pillai, P. Mukundan, K.G.K. Warrier, Sol–gel synthesis of nanosized anatase from titanyl sulfate, Mater. Lett. 57 (2002) 330–335.
[29] R.K. Wahi, Y.P. Liu, J.C. Falkner, V.L. Colvin, Solvothermal synthesis and characterization of anatase TiO_2 nanocrystals with ultrahigh surface area, J. Colloid Interface Sci. 302 (2006) 530–536.
[30] T. Ohsaka, F. Izumi, Y. Fujiki, Raman spectrum of anatase, TiO_2, J. Raman Spectr. 7 (1978) 321–324.
[31] T. Ohsaka, Temperature dependence of the Raman spectrum in anatase TiO_2, J. Phys. Soc. Jpn. 48 (1980) 1661–1668.
[32] C.Y. Xu, P.X. Zhang, L. Yan, Blue shift of Raman peak from coated TiO_2 nanoparticles, J. Raman Spectrosc. 32 (2001) 862–865.
[33] K.R. Zhu, M.S. Zhang, Q. Chen, Z. Yin, Size and phonon-confinement effects on low-frequency Raman mode of anatase TiO_2 nanocrystal, Phys. Lett. A 340 (2005) 220–227.
[34] P.C. Ricci, M. Salis, A. Anedda, Phonon characterization of nano-crystals by Raman spectroscopy, Chem. Phys. Lett. 457 (2008) 191–193.
[35] K. Mogyorósi, I. Dékány, J.H. Fendler, Preparation and characterization of clay mineral intercalated titanium dioxide nanoparticles, Langmuir 19 (2003) 2938–2946.
[36] E. Murad, H.M. Koester, Determination of the Ti speciation in commercial kaolins by Raman spectroscopy, Clay Miner. 34 (1999) 479–485.
[37] T. Xu, Y. Cai, K. O'Shea, Adsorption and photocatalyzed oxidation of methylated arsenic species in TiO_2 suspensions, Environ. Sci. Technol. 41 (2007) 5471–5477.
[38] C. Jing, S. Liu, X.G. Meng, Arsenic remobilization in water treatment adsorbents under reducing conditions: part I. Incubation study, Sci. Total Environ. 389 (2008) 188–194.
[39] M. Anpo, T. Shima, S. Kodama, Y. Kubokawa, Photocatalytic hydrogenation of CH_3CCH with H_2O on small-particle TiO_2: size quantization effects and reaction intermediates, J. Phys. Chem. 91 (1987) 4305–4310.
[40] C. Kormann, D.W. Bahnemann, M.R. Hoffmann, Preparation and characterization of quantum size titanium dioxide (TiO_2), J. Phys. Chem. 92 (1988) 5196–5201.
[41] L.E. Brus, Electron–electron and electron–hole interaction in small semiconductor crystallites, the size dependence of the lowest excited electronic state, J. Chem. Phys. 80 (1984) 4403–4409.
[42] L. Brus, Electronic wave functions in semiconductor clusters: experiment and theory, J. Phys. Chem. 90 (1986) 2555–2560.
[43] S. Liu, N. Jaffrezic, C. Guillard, Size effects in liquid-phase photo-oxidation of phenol using nanometer-sized TiO_2 catalysts, Appl. Surf. Sci. 255 (2008) 2704–2709.